

Final Report
NASA Grant #NAG8-160

1N-34-CR

5 CIT

186109

27P

**Droplet-Turbulence Interactions in Sprays Exposed to
Supercritical Environmental Conditions**

Principal Investigator: Domenic A. Santavicca
Penn State University
(814)863-1863

NASA Technical Officer: Klaus N. Gross
MSFC - EP55
(205)544-2262

(NASA-CR-194408)
DROPLET-TURBULENCE INTERACTIONS IN
SPRAYS EXPOSED TO SUPERCRITICAL
ENVIRONMENTAL CONDITIONS Final
Report (Pennsylvania State Univ.)
27 p

N94-14308

Unclas

G3/34 0186109

September 1993

Table of Contents

	<u>Page</u>
Title Page	i
Table of Contents	ii
Introduction	1
Major Accomplishments	2
Droplet-Turbulence Interactions in Dilute Sprays (E. Coy)	3
Exciplex Thermometry (S. Greenfield)	7
Raman Imaging of Supercritical Droplets and Jets (T. Spegar)	12
An Experimental Study of Droplet Motion in Laminar and Highly Turbulent Flows (Y.-H. Song)	16
Droplet Vaporization in an Acoustic Field (M. Ondas)	21
Publications	25
Personnel	25

Introduction

The goal of this research has been to experimentally characterize the behavior of droplets in vaporizing sprays under conditions typical of those encountered in high pressure combustion systems such as liquid fueled rocket engines. Of particular interest are measurements of droplet drag and lift, droplet dispersion, droplet heating, and droplet vaporization under both subcritical and supercritical conditions.

This report includes a summary of the major accomplishments achieved under NASA Grant #NAG8-160 during the period from June 1990 through June 1993, a brief description and status report on five research areas, which have been directly or indirectly supported by this grant, and a list of publications and personnel associated with this research. (Note that the names in parentheses following the research area headings refer to the graduate student associated with that particular project.)

Major Accomplishments

NASA Grant #NAG8-160

June 1990 - June 1993

1. Four unique flow systems were designed and constructed for the purpose of studying droplet-turbulence interactions at subcritical and supercritical conditions. The operating characteristics of these four systems are as follows:
 - 500 K, 50 m/sec, 1 atm
 - 500 K, 10 m/sec, 10 atm \pm 10% at 100-1000 Hz
 - 500 K, 10 m/sec, 70 atm
 - 500 K, 1 m/sec, 150 atm
2. A droplet imaging velocimetry technique has been developed for making simultaneous droplet size and velocity measurements in dilute sprays. This work was presented at the 27th JANNAF Combustion Meeting and at the 1991 SAE Fuels and Lubricants Meeting.
3. A 2-D Raman imaging system has been developed, and the feasibility of applying it to study droplet behavior in supercritical environments has been demonstrated.
4. An exciplex fluorescence-based droplet thermometry technique has been developed and calibrated.
5. A high pressure, cryogenic droplet generator has been successfully developed for studying liquid nitrogen jets and droplets in supercritical environments.
6. A study of drag and lift forces acting on an evaporating droplet along a curvilinear trajectory has been conducted. This work will be presented at the 1993 ESSCI Fall Meeting.
7. A study of droplet drag in highly turbulent flows has been conducted. This work will be presented at the 1993 ESSCI Fall Meeting.

Droplet -Turbulence Interactions in Dilute Sprays (E.B. Coy)

Some preliminary experiments have been performed on the motion of droplets in the self-generated turbulence of a spray. The experimental conditions were chosen to isolate the role of drop size on the development of sprays. This was accomplished by operating three different size atomizers in the Delavan WDB series at the same thrust level and measuring the droplet number density as a function of size position and velocity along a radius 5 cm from the nozzle exit. The following results demonstrate the capability of the measurement technique for determining the size-velocity correlation.

Experiments involving the motion of droplets are performed in either the Eulerian frame (stationary), or the Lagrangian frame (following individual droplets). Due to the high number density of droplets in sprays following individual droplets over a significant portion of their lifetime is a practical impossibility, therefore experiments in sprays are always conducted in the Eulerian frame. The experimental technique discussed below has been developed for obtaining drop size and velocity information in dilute sprays.

A schematic drawing of the apparatus is shown in fig. 1. It is basically an adaptation of the particle image velocimetry (PIV) technique¹. The laser beams are focused into sheets which coincide with the image plane of the camera. The camera shutter is opened and the lasers are fired in rapid succession forming two distinct images of each droplet. The two components of droplet velocity in the image plane are determined from the displacement of the images and the time interval between pulses. A typical image contains many droplets and correctly matching them is not trivial. The matching is facilitated if the the droplet images formed by the two laser pulses can be distinguished by color. This was accomplished by doping the liquid with two fluorescent dyes (e.g., Rhodamine 610 and Stilbene 420) and these dyes are excited with the second and third harmonics, respectively, of two Nd:YAG lasers. The dyes were chosen based on their absorption and emission spectra. Rhodamine 610 absorbs at the second harmonic (532 nm) and emits at 610 nm while Stilbene 420 absorbs at the third harmonic (355 nm) and emits at 420 nm. These characteristics permit the intense elastic scattering of the excitation wavelengths to be eliminated with a narrow band mirror and edge filter thus permitting only the fluorescent emission from the droplets to be captured on 35mm color slide film. The images are recorded at 2:1 magnification which gives a field of view of 18 mm by 12 mm. The film used is ASA 200 color reversal film (e.g., Kodak Ektachrome 200).

The slides are automatically analyzed using a microcomputer based image processing system.

The microcomputer is an 80386-25 MHz and the frame grabber is a 512x480, 256 gray levels, Data

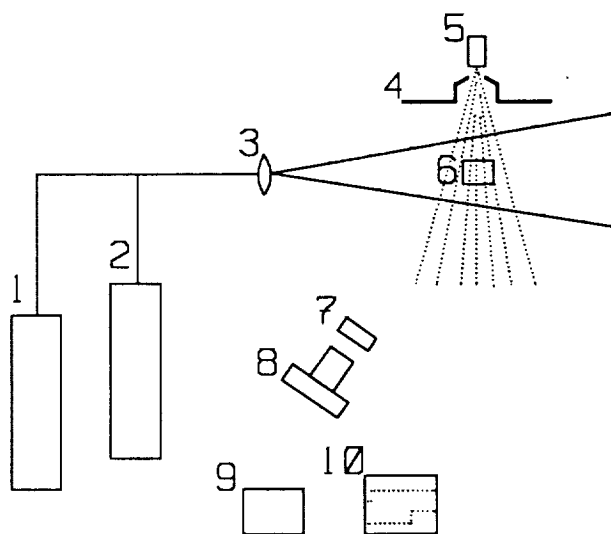


Fig. 1 1-355nm beam, 2-532nm beam, 3-light sheet optics, 4-skimmer, 5-nozzle, 6-sample volume, 7-532nm mirror, 8-35mm camera, 9-timing circuit, 10-oscilloscope

Translation, DT2851-60Hz. The slides are placed in a translation stage system which positions the slide relative to an RS-170, CCD camera and allows the slide to be analyzed in 225 fields, 2.4 mm wide by 1.6 mm high. For each field an image of the blue droplets is obtained by interposing a bandpass filter between the quartz-halogen lamp and the slide. The digitized image is scanned and the droplets are located and sized. The process is repeated for the red droplets. The drop size and position are stored for post processing for velocity. The time required to analyze a single slide containing about 1000 droplet images is about 25 minutes.

Results The following results show that the desired operating conditions have been achieved and also demonstrate the capability of the droplet imaging technique for measuring the joint distribution function of size, position and velocity.

A. **Thrust** Fig. 2. shows the thrust vs. pressure relationship for four Delaven WDB series atomizers. The reaction force was measured by supporting the nozzle on a three-beam balance. The upper limit of the range of acceptable operating pressures is constrained by the desired range of drop sizes. Increasing pressure decreases drop sizes for a given nozzle. The lower limit is constrained by the supply pressure necessary for good atomization which is about 3.5×10^5 Pascals. A thrust of 0.075 Newtons was chosen as the optimum operating condition for nozzles 4, 5 and 6.

B. **Mass Flow** The mass flow at 0.075 Newtons was measured for each nozzle by collecting and weighing the discharge. The collection efficiency was at least 98% as determined by returning the discharged liquid to the supply system and repeating the test. The mass flows are shown in fig. 2. From the measured mass flow and thrust it was possible to calculate an average exit axial velocity for the three nozzles. These are given in table 1.

C. **Droplet Image Velocimetry Data** Droplet image velocimetry measurements were made along a radius 5 cm below the nozzle exit for each of the three nozzles. There are five independent variables so it is not possible to succinctly represent all the data. An important phenomena affecting the measurements is expansion of the beam as it penetrates the spray due to diffraction. This was not recognized when the measurements were made for the WDB 4.0 nozzle and the measurements were made on the opposite side of the spray from the entrance point of the laser sheet.

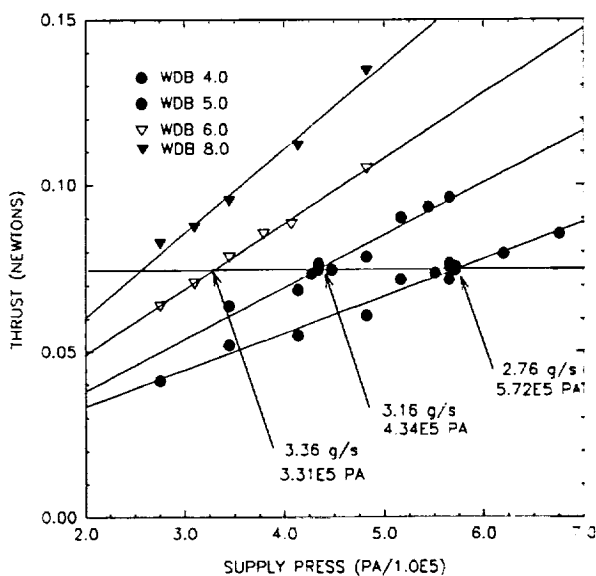


Figure 2 Nozzle thrust vs. supply pressure for four Delaven WDB series swirl atomizers.

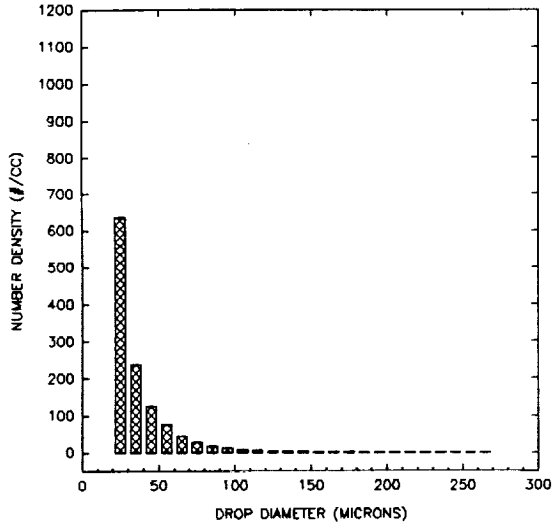


Figure 3 Droplet number density vs. drop diameter averaged over radius at axial position of 5 cm for WDB 4.0 atomizer.

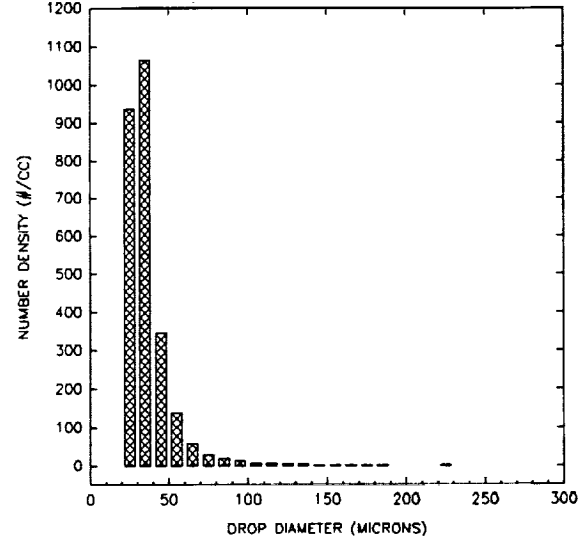


Figure 4 Same as figure 3. for WDB 5.0 atomizer.

Since the mass flow was known independently it was possible to estimate the effective width of the sample volume using the measured distribution function. The effective width is given as W_{EFT} in the table. Using W_{EFT} it was possible to calculate an integrated momentum of the droplets at the measurement location, T_{DID} , which is also given in table 1.

D. Size Distributions The droplet size distributions for the three atomizers are given in figures 3, 4 and 5. These distributions are integrated over the radius.

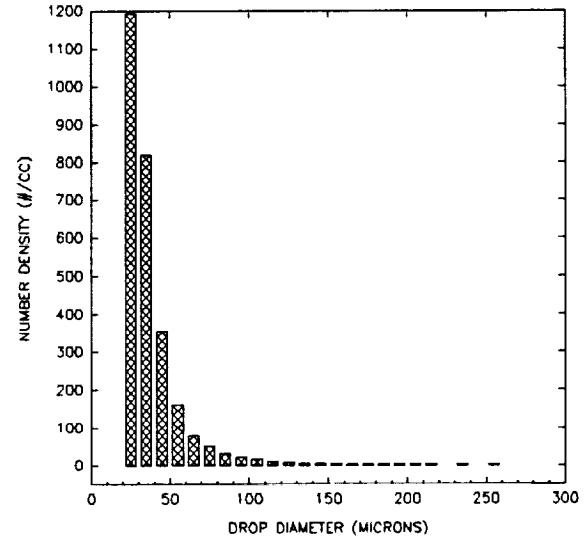


Figure 5 Same as figure 3. for WDB 6.0 atomizer.

Table 1

WDB	NUMBER	Q (cm ³ /s)	V _{EXIT} (m/s)	W _{EFF} (mm)	T _{WID} (N)
4.0	12939	3.48	27.2	5.8	0.069
5.0	7719	3.98	23.8	1.8	0.071
6.0	15237	4.24	22.3	2.0	0.075

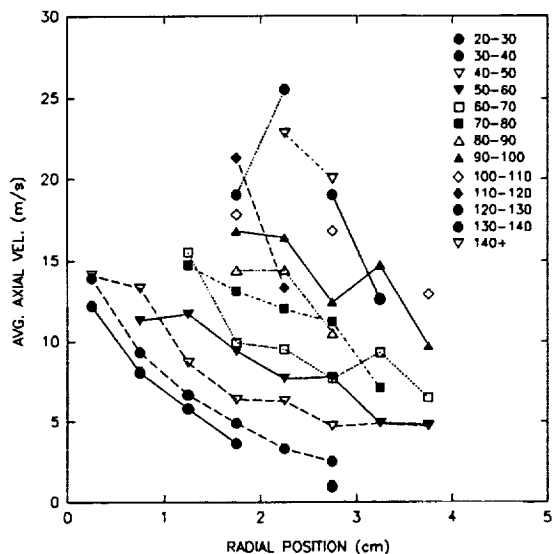


Figure 6 Average velocity as function of radial position for several size ranges of droplets for WDB 4.0 atomizer.

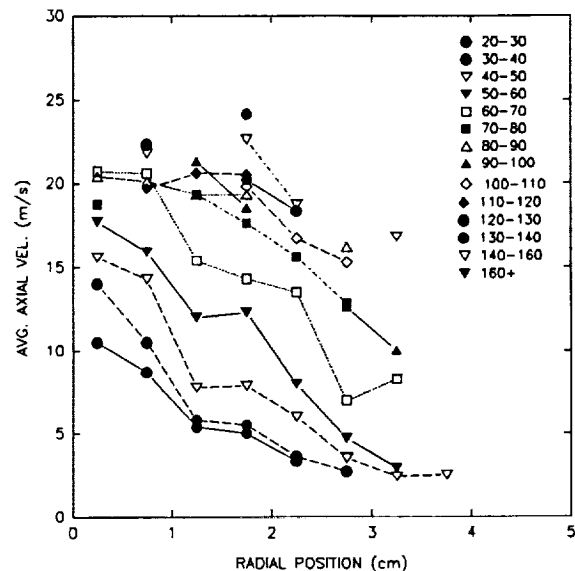


Figure 7 Same as figure 6. for WDB 5.0 atomizer.

Virtually all the droplets are less than 200 μm which is the size which was identified as an upper limit for neglecting the effects of gravity since the terminal velocity of a 200 μm methanol droplet is 0.5 m/s.

2. Size-Velocity Correlations: Average axial velocity as a function of radial position for the range of droplet sizes is shown in figures 6, 7, and 8. It appears that larger samples will be required to achieve smooth velocity profiles; however, the trends with respect to drop size and radial position are evident and the velocities of the largest droplets agree favorably with the initial exit velocity based on thrust and mass flow. The large droplets are clustered about the two cm radial position indicating that the initial direction acquired at the breakup of the cone has not been significantly modified by the gas flow. The large droplets also are traveling at velocities approaching the outlet velocity. Small droplet velocities have already assumed the characteristic Gaussian profile of a turbulent jet.

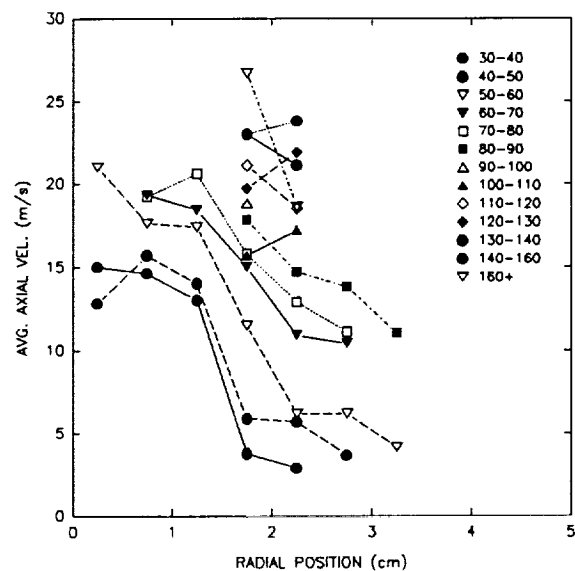


Figure 8 Same as figure 6. for WDB 6.0

References

1. Adrian, R.J., Multi-point Optical Measurements of Simultaneous Vectors in Unsteady Flow - A Review, Int. J. Heat and Fluid Flow, 1986

Exciplex Thermometry (S.C. Greenfield)

Measurement of droplet temperature is important because of its influence on droplet vaporization, e.g., droplet models require droplet temperatures to accurately predict vaporization rates. Most prior experiments involved the suspension of a droplet on a thermocouple,^{1,2,3,4} however, this introduces several uncertainties into the results due to heat conduction through the suspension device, asphericity of the droplet, and disruption of both the internal and external flowfields of the droplet. Exciplex thermometry has the advantage of being a non-intrusive fluorescence technique, thus eliminating the forementioned problems.

Figure 1 shows the major components of a system that has been set up to experimentally measure droplet temperatures. It includes a frequency tripled (355 nm) Spectra-Physics Nd:YAG laser (maximum 60 mJ/pulse, 10 Hz), a Princeton Instruments 14-bit, intensified, cooled, 384 x 578 pixel CCD camera, and a droplet generator. The main test section also contains a turbulence generator⁵ capable of 40% relative turbulence intensities. Droplet production is performed with an aerodynamic droplet generator⁶ which is detailed in Figure 2. This design is based on a simple balance of the surface tension and aerodynamic drag forces on the droplet. Variation of the fuel flow rate, nitrogen flow rate, tip tubing size, and tip wire diameter can all be used to vary the droplet size and frequency.

The exciplex system chosen for this experiment was 2.5% (by weight) tetramethyl-1,4-phenylene-diamine (TMPD) and 1.0% 1-methylnaphthalene (1MN) in tetradecane (TD). The laser was used as an excitation source for the TMPD (the other components are non-absorbing at this wavelength). The TMPD^{*} then undergoes one of two major processes: it may simply return to the ground state, fluorescing at approximately

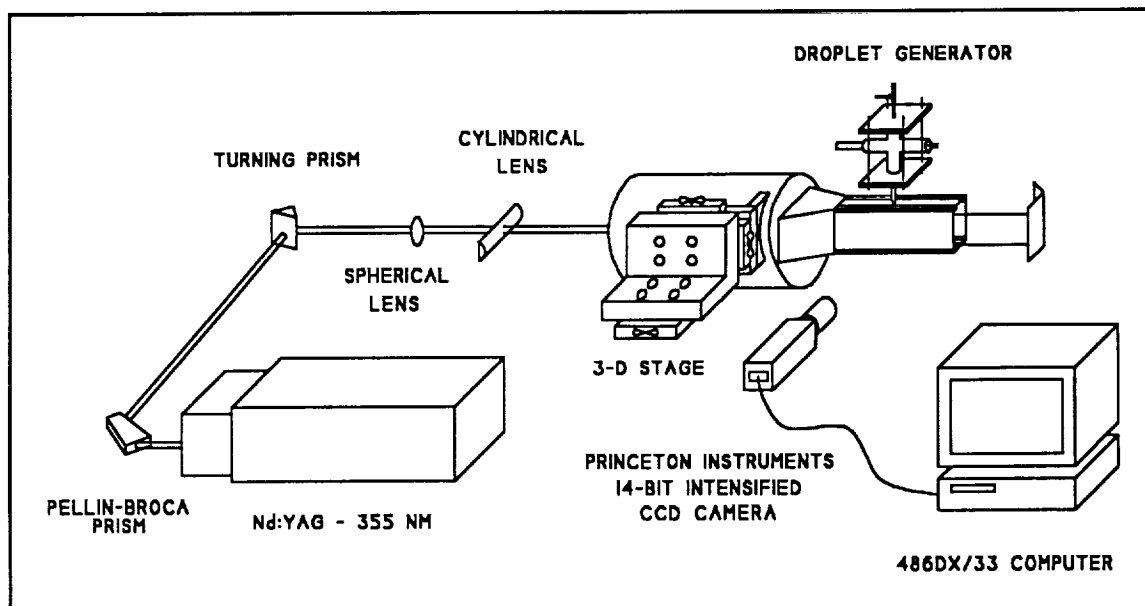


Figure 1. Experimental Apparatus for Droplet Production and Exciplex Imaging.

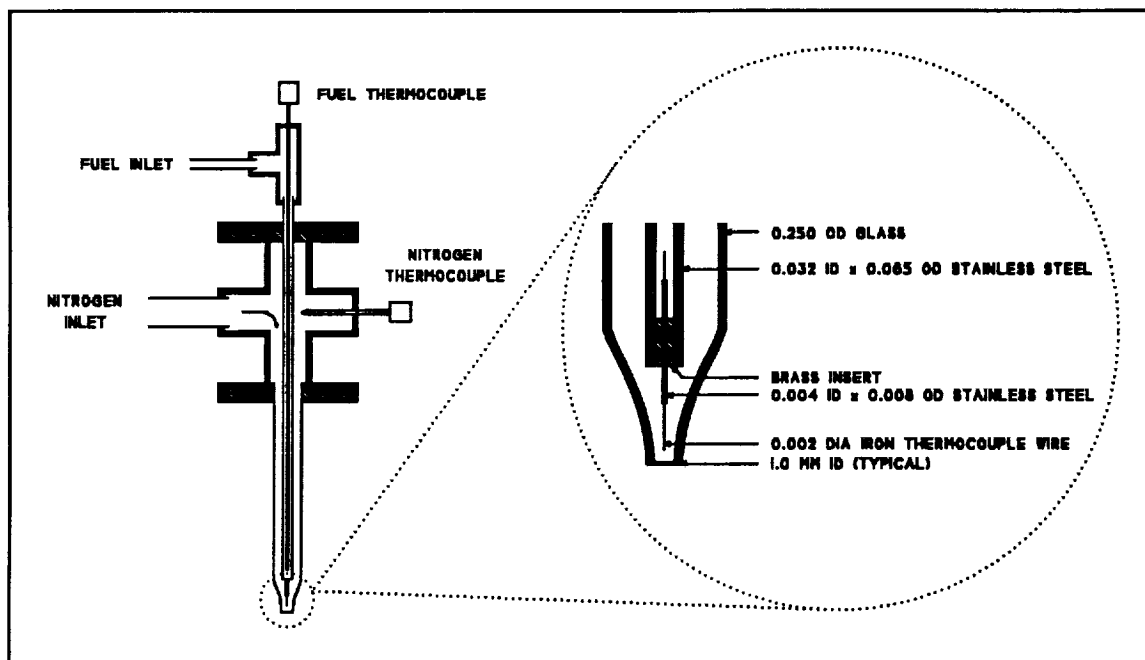


Figure 2. Aerodynamic Droplet Generator.

400 nm (monomer fluorescence), or it may bind to a 1MN molecule to form an exciplex:^{7,8,9}



This new molecule will then return to the ground state, fluorescing at approximately 500 nm (exciplex fluorescence). This fluorescence is red-shifted relative to the monomer fluorescence because energy was required to bind the molecules together (see Figure 3). The ratio of intensities at these two wavelengths is temperature-dependent and, upon calibration, can be used as a thermometer. These chemicals were chosen for both their exciplex-forming capabilities and because their boiling points are well-matched (TMPD-260°C, 1MN-242°C, TD-252°C). This is important because the intensity ratio versus temperature curve is concentration-dependent, i.e., differential component vaporization would bias the measurements, especially at elevated temperatures.

Separation of the two fluorescence signals was performed with a split-image filter and bandpass filters. The split-image filter (SIF) simply produces two images of one object. One bandpass filter, a Corion S40-400 (centered at 400 nm, 40 nm FWHM), is placed behind one half of the SIF and transmits the monomer fluorescence. The second, a

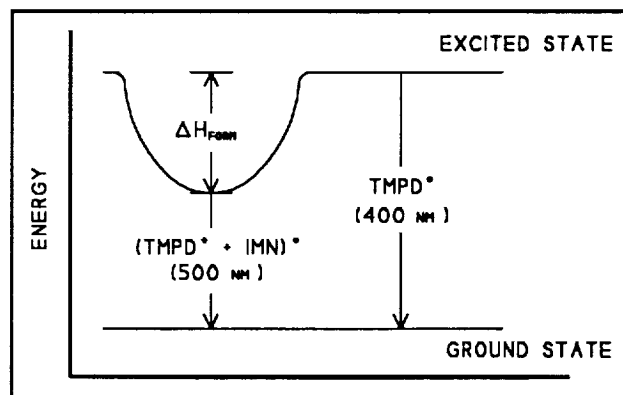


Figure 3. Exciplex Energy Level Diagram.^{7,9}

Corion S25-500 (centered at 500 nm, 25 nm FWHM), is placed behind the other half of the SIF and transmits the exciplex fluorescence. Additionally, a 385 nm high-pass filter (Melles-Griot 03FCG049, i.e., Schott GG385) was required for complete elimination of the 355 nm laser scattering.

Many attempts were made to produce a calibration curve using droplets of known temperature. Unfortunately, wide variability existed in the intensity ratio measurements of droplets presumably at the same temperature. Three of the most probable causes of this variability can be identified. First, even though the droplets were preheated for isothermal injection into the surrounding environment, vaporization would still cool the droplets; thus, the exact temperature was uncertain. Second, the purchased TMPD showed a fairly high degree of oxidation, which may affect the measured intensity ratios and repeatability of the experiments, although the quantitative effects are not yet fully known. Finally, there appears to be a viewing angle affect resulting from the use of the split-image filter to simultaneously image the exciplex and monomer fluorescence. Because a droplet is three-dimensional and not planar, the two images appear to emanate from different parts of the droplet, the left image biased towards the front of the droplet and the right towards the back. Thus, as the droplet location changes from left to right, the region that is imaged changes as well. Since the fluorescence is more intense on the front face (i.e., in the optically thick case, where the laser first contacts the droplet), the intensity ratio will be biased by the droplet location within the field of view.

To circumvent these problems, a new experiment was designed. Instead of droplets, an Amersil T08 quartz tube (1 mm ID, 2 mm OD) containing a thermocouple was used for calibration purposes. This tubing was chosen because it does not fluoresce when hit by the 355 nm beam and for its excellent transmission properties over the entire spectral range of interest.

A 120 μm pinhole was placed in front of the tubing to prevent image overlap (caused by the split-image filter) during acquisition. Additionally, a sublimation unit was purchased to purify the TMPD. An initial set of calibration data was acquired with the Princeton Instruments intensified CCD camera and is shown in Figure 4.

The results of this experiment were quite encouraging. Although double-valued in nature, the curve shows excellent sensitivity (i.e., has a large slope) in both the low and high temperature regions, the only problematic area falling in the 90° to 115°C range. Because it was an initial experiment, several minor problems occurred that have since been corrected. This data will be retaken and is expected to be smoother and more repeatable (i.e., at a given

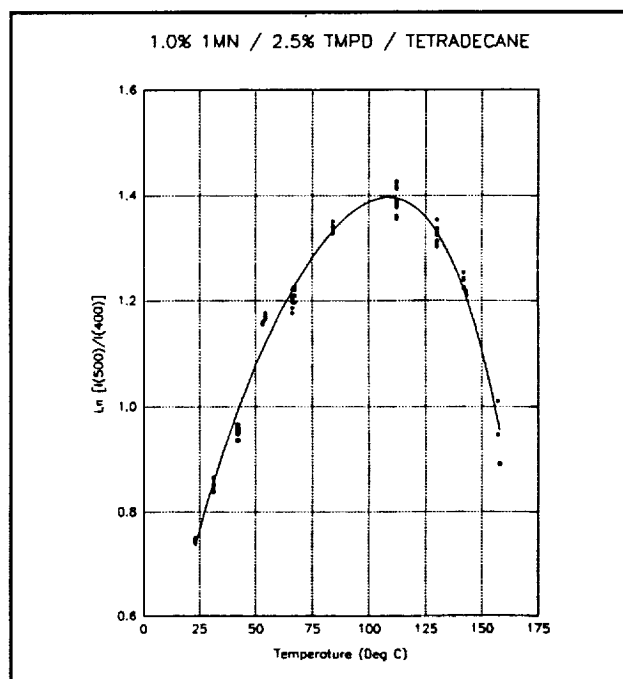


Figure 4. Exciplex Calibration Curve: Ln(Intensity Ratio) Versus Temperature.

temperature) than that presented in Figure 4.

Several other experiments will be run for verification purposes. First, the data will be checked for repeatability by taking the calibration data under both heat-up and cool-down conditions. This will also verify that heating the mixture does not induce any chemical alterations of the system. Second, calibration curves will be produced for several other combinations of exciplex concentrations. This serves a dual purpose: by varying concentrations, one can alter the optical density of the system, thus allowing for a variety of volume-averaged temperature measurements, and it will allow for an estimation of the errors induced by differential vaporization which may be occurring at the elevated temperatures, i.e., to account for concentration changes.

By acquiring the volume-averaged droplet temperatures from several regions of the droplet, a comparison can be made to determine the level of mixing within the droplet. However, another set of experiments must be run to verify that the fluorescence from the region of interest is not inducing large levels of fluorescence in other droplet regions, which would affect the temperatures being measured, i.e., one would no longer be able to study various temperature regions by changing the optical density of the solution. This experiment will involve using a narrow slit (e.g., 10 μm) to observe intensity levels as a function of path length through the exciplex solution in a quartz cell. Comparison of this data to that of the measured absorption path length will show how much the induced fluorescence of these regions will bias the temperature data.

Finally, a droplet acts as a lens for both the incoming laser light and the outgoing fluorescence signals. Because the index of refraction is a function of wavelength, the light will be refracted differently at the surface. Therefore, it must be verified that the droplet lensing effect does not alter the intensity ratio for a given temperature. This will be checked in two separate ways. First, a set of calibration data using droplets will be taken at low temperatures, e.g., 22°-50°C, and be compared to the calibration data taken with quartz tubing. Additionally, a computer model developed by Coy¹⁰ will be used to observe how the two fluorescence signals will be imaged onto the CCD camera. If the two images appear similar, it will be further verification that the droplet does not affect the observed intensity ratio. Once verification is complete, experimental droplet temperatures will be measured using the exciplex technique.

References

1. Ranz, W.E., and Marshall, W.R., Jr., "Evaporation From Drops - Part I," *Chemical Engineering Progress*, Vol. 48, No. 3 (1952), p.141.
2. Ranz, W.E., and Marshall, W.R., Jr., "Evaporation From Drops - Part II," *Chemical Engineering Progress*, Vol. 48, No. 4 (1952), p.173.
3. Charlesworth, D.H., and Marshall, W.R., "Evaporation From Drops Containing Dissolved Solids," *AIChE J.*, Vol. 6, No. 1, (1959), p.9.
4. Trommelen, A.M., and Crosby, E.J., "Evaporation and Drying of Drops in Superheated Vapors," *AIChE J.*, Vol. 16, No. 5, (1970), p.857.

5. Videto, B.D., and Santaviccà, D.A., "A Turbulent Flow System for Studying Turbulent Combustion Processes," *Combust. Sci. Tech.*, Vol. 76 (1991), p.159.
6. Green, G.J., Takahashi, F., Walsh, D.E., and Dryer, F.L., "Aerodynamic Device for Generating Mono-disperse Fuel Droplets," Proceedings, Eastern States Section of the Combustion Institute, 1988, p.96-1.
7. Melton, L.A., "Quantitative Use of Exciplex-Based Vapor/Liquid Visualization Systems (A Users Manual)," Final Report, Army Research Office Contract DAAL03-86-K-0082, 1988.
8. Murray, A.M., and Melton, L.A., "Fluorescence Methods for Determination of Temperature in Fuel Sprays," *Applied Optics*, Vol. 24, No. 17 (1985), p.2783.
9. Melton, L.A., Murray, A.M., and Verdick, J.F., "Laser Fluorescence Measurements for Fuel Sprays," *SPIE Symposium Series, Remote Sensing*, Vol. 644, p.40.
10. Coy, E.B., In-house PC-based computer program.

Raman Imaging of Supercritical Droplets and Jets (T. Spegar)

In liquid propellant rocket engines, the behavior of the injected liquid highly influences the subsequent combustion process. Often the combustion chamber pressure and temperature exceed the critical pressure and temperature of the injected fuel and/or oxidizer. Transport processes in the spray dictate how the temperature of the droplets will change. Since the temperature of the combustion chamber surpasses the liquid temperature at injection, one might expect the liquid temperature to increase and approach the surrounding temperature. However, conditions may exist where the vaporization rate is so high that the droplet temperature decreases or total vaporization is achieved before the droplet reaches its critical temperature. But if the droplet approaches or exceeds its critical temperature, the corresponding decrease in surface tension will play an important role in droplet behavior. Namely, droplet distortion, breakup, vaporization rate and drag, as well as enhanced permeation of the surrounding environment, can be significantly affected by a decrease or absence of surface tension. The objective of this work is to experimentally investigate these fluid phenomena in the helium-nitrogen binary system.

Helium and nitrogen have highly dissimilar critical temperatures and pressures, much as the differences between hydrogen and oxygen:

	T_c (K)	P_c (MPa)
He	5.3	0.23
N ₂	126.2	3.39
H ₂	33.3	1.30
O ₂	154.8	5.08

Thus, to a first approximation, one might expect similar phase behavior characteristics between these two binary systems.

A more thorough comparison can be made by using the approach of Van Konynenburg and Scott.¹ The individual components of each system are assumed to obey the Van der Waals equation of state. The Van der Waals constants a_{11} , a_{22} , b_{11} , and b_{22} , and mixture parameters a_{12} and b_{12} are calculated using the individual component critical properties and appropriate mixing rules. The mixtures are distinguished by three dimensionless constants ξ , ζ , and Λ , and were evaluated for the two systems using measured critical constants for hydrogen and helium. But, since hydrogen and helium are small in size, quantum effects can become important, and in an attempt to correct for this, modified critical pressure and temperature values were used.² With the exception of one case, the parameters indicated the same qualitative type of behavior classified as type III³. In the one exception, behavior differs mainly at lower pressures and temperatures, i. e. those approaching the critical pressure and temperature of the more volatile component. No binary system can perfectly mimic the behavior of another system, and although the above technique is not rigorous, it offers an added validity to the

choice of components and importance of results.

Spontaneous Raman scattering is a most effective diagnostic technique due to its species selectivity and linear dependence on species concentration. In fact, helium is Raman inactive and thus the Raman signal is entirely due to nitrogen in the mixture. Since the intensity of the Raman signal scales with signal frequency to the fourth power, it is desirable to use high frequency laser light for excitation. Coumarin 504 laser dye was chosen for its relatively low lasing wavelengths and high gain characteristics, and was found to lase most intensely at 512 nm. The Raman frequency shift for nitrogen is $\Delta\nu = 2331 \text{ cm}^{-1}$, and with laser excitation of 512 nm, the Stokes Raman vibrational signal occurs at approximately 581 nm.

Figure 1 shows a cross-sectional view of the high pressure test chamber. In the past, the chamber was mounted 90° from its current position with the droplet generator inserted downward through the end where the laser sheet now enters. Droplets were injected into a downward co-flow of helium. However, the droplet

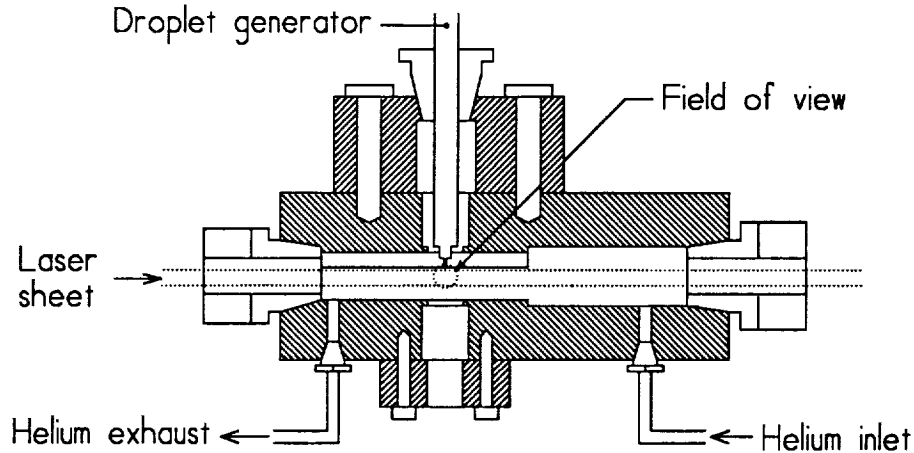


Figure 1. Test chamber cross-sectional view.

generator, being cool itself, produced density gradients in the helium flow which greatly disturbed flow conditions in the field of view. In the current configuration, the helium crossflow is introduced from right to left, into which the liquid jet is transversely injected. The crossflow has the effect of flushing the field of view of nitrogen with ambient temperature helium at a low velocity. The velocity can also be increased to study the effects of a strong crossflow. The jet issues through a 0.004" ID stainless steel tubing into a 0.5" field of view where images are taken. The laser sheet is transmitted through end windows antiparallel to the helium flow.

Figure 2 is a schematic of the entire experimental apparatus. The focusing optics reduce the laser beam diameter and produce a vertical laser sheet. The image is viewed by a Princeton Instruments intensified CCD camera with a 60 mm Nikon lens. A narrow bandpass filter centered at the Raman wavelength along with a high-pass filter reject noise from the laser excitation, dye fluorescence and flashlamp light. To create a liquid nitrogen jet, liquid nitrogen at low pressure flows into the droplet generator, circulates down to within 1.0" from

the point of injection, and then exhausted. The bath of liquid nitrogen keeps the entire droplet generator cool to minimize thermal stresses. High pressure gaseous nitrogen flows into the droplet generator, is condensed by

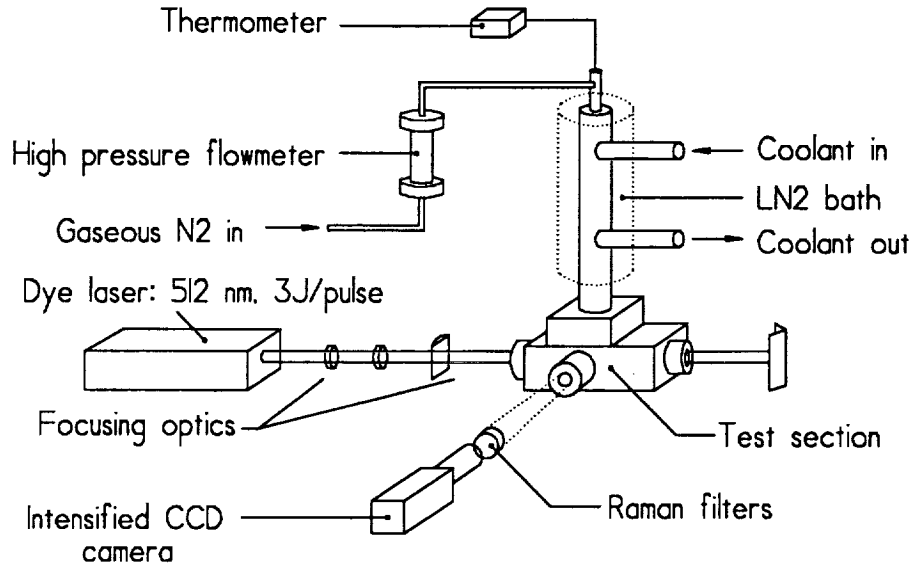


Figure 2. Experimental apparatus.

the coolant, and is thus injected as a liquid. The liquid temperature is monitored by a thermocouple positioned at 0.75" from the tip. Although it is possible to measure the concentration of nitrogen at the chamber exhaust to deduce the jet velocity, it is in principle easier to measure nitrogen flow before injection. The high pressure flowmeter is a low-flow rotameter enclosed in a pressure vessel to prevent bursting of the tube, and has been calibrated for high pressures.

Figure 3 is an image of a liquid nitrogen jet back-lighted with a strobe light and acquired with the

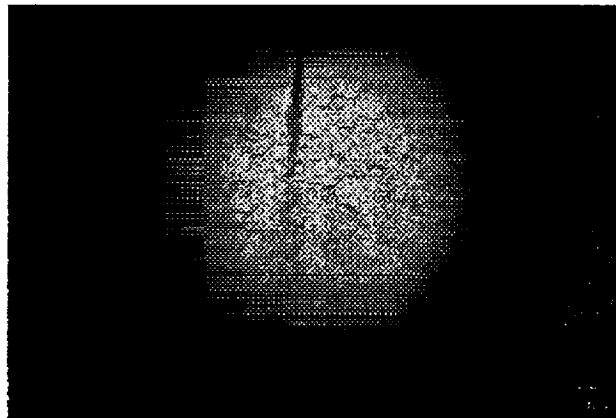


Figure 3. Liquid nitrogen jet in a supercritical environment.

CCD camera. The field of view diameter is approximately 0.5" and the jet diameter is 0.004". The ambient helium environment is at room temperature and at about 900 psig, well above the nitrogen critical temperature

of 126.2 K and critical pressure of 492 psi. Notice that the jet is characteristic of an atomizing liquid spray, however there is no evidence of liquid droplets. The jet appears to be liquid at the orifice but appears gaseous at the bottom of the field of view. This has been observed by others and its characteristics have been compared with those of a turbulent submerged jet⁴. Observations show that pressure plays an important role in jet behavior.

Raman scattering measurements have been initiated to determine relative nitrogen concentrations in the jet and droplet wakes at various conditions. It was determined that the laser flashlamps and dye fluorescence produce some light at the Raman wavelength which overcomes the weak Raman signal. Hence, a laser mirror has been obtained to reject the unwanted noise before the laser sheet passes through the test chamber. Also, density gradients downstream of the injection point tend to perturb the laser sheet profile, whose effect is magnified by the time the sheet passes through the field of view. The setup will be modified to pass the sheet through the test chamber in the same direction as the helium flow.

Nitrogen concentration measurements may be possible within the jet and droplets themselves. This is much more difficult than wake measurements since elastic scattering from the liquid surface may be present and may be impossible to filter without losing the Raman signal. The technique possibly can be accomplished if the liquid surpasses its critical temperature causing the surface to no longer be well defined.

References

1. Van Konynenburg, P.H., and Scott, R.L., "Critical Lines and Phase Equilibria in Binary Van Der Waals Mixtures," *Royal Society of London Philosophical Transactions*, Ser. A, Vol. 298 (1980), 495-540.
2. Gunn, R. D., Chueh, P. L., and Prausnitz, J. M., "Prediction of Thermodynamic Properties of Dense Gas Mixtures Containing One or More of the Quantum Gases," *A.I.Ch.E. J.*, Vol. 12, No. 5 (1966), 937-941.
3. Rowlinson, J. S., and Swinton, F. L., *Liquids and Liquid Mixtures*, 3rd ed. (Butterworth & Co., Ltd., London, 1982).
4. Newman, J. A., and Brzustowski, T. A., "Breakup of a Liquid Jet in a High-Pressure Environment," *A.I.A.A. J.*, Vol. 8, No. 1 (1970), 164-165.

An Experimental Study of Droplet Motion in Laminar and Highly Turbulent Flows (Y.-H. Song)

Introduction

The objective of this study is to experimentally study the motion of droplets undergoing unsteady curvilinear motion in laminar and turbulent flows. Droplet or particle motion has been studied for a long time, and some aspects of droplet motion are well understood. For example, for a non-vaporizing solid sphere undergoing steady rectilinear motion in a laminar flow, the standard drag curve and the steady equation of motion can be used to accurately predict the sphere's velocity and trajectory. However, for the case of droplet motion in actual spray combustion systems, where vaporization, unsteady curvilinear motion and free-stream turbulence must also be accounted for such behavior is not well understood. In order to study these effects on droplet motion, small (90-300 μm) single droplets were transversely injected into an air flow which can be laminar or highly turbulent flows (up to 40% relative turbulence intensity), with various pressure and temperature conditions. The investigated droplet Reynolds numbers in this study range from 10 to 500, which covers typical droplet Reynolds numbers in spray combustion systems.

Experimental Approach

Single droplet experiments are performed in a high temperature and pressure facility, illustrated schematically in Figure 1. This system is capable of operating at pressures up to 70 atm and temperatures up to 600 K. The flow passage in the test section is 19 mm in height and 12.7 mm wide. In order to obtain turbulence intensities which are representative of spray combustion systems, i.e. up to 40 %, a novel turbulence generator (Videto and Santavicca 1991) which is capable of producing isotropic, homogeneous turbulence with intensities as large as 80 % was used. For the laminar experiments, the turbulence generator can be simply replaced with a flow straightener which produces laminar flow with a uniform velocity profile. An aerodynamic droplet generator is used in this study. The droplet diameter can be controlled with this device over a range of 50-300 μm . The frequency of droplet generation can be varied from 1 to 60 Hz depending on droplet size. Typically, each droplet is separated by 200 droplet diameters in the test section, which insures that there are no droplet-droplet interactions.

An argon ion laser is used to illuminate the droplets. The laser beam is mechanically chopped at 833 Hz or 1000 Hz to obtain a time resolved droplet trajectory that is recorded on 35 mm slide film. Droplet velocity and acceleration are obtained directly by first and second finite differentiation, respectively. Droplet size measurements are obtained using a strobe to backlight the droplets and recording the droplet images at high magnification with a CCD video camera system.

Results

The Effect of Evaporation, Unsteady Motion, and Curvilinear Motion on Droplet Drag

In order to investigate the effects of evaporation, unsteady motion, and curvilinear motion on droplet drag, evaporating droplets undergoing curvilinear motion were investigated in a laminar flow. The experimentally obtained drag coefficients, without and with correcting for vaporization, are compared with the standard drag correlation in Figures 2-a and 2-b, respectively. The standard drag correlation used in this work was suggested by Clift, Grace and Weber (1978). In Figure 2-a, the droplet Reynolds numbers are calculated using the free stream air density and viscosity. In Figure 2-b, the droplet Reynolds numbers are estimated using the 1/3 rule, and the measured drag coefficients are multiplied by $(1+B)^{0.32}$, as proposed by Chiang, Raju and Sirignano (1992) to correct for vaporization. Figure 2-a shows that the drag coefficients of evaporating droplets are significantly reduced as the air temperature increases. As shown in Figure 2-b, if the effect of vaporization on drag is included, the measured drag coefficients agree well with the standard drag curve. Because the standard drag curve was developed for steady rectilinear motion of a non-vaporizing solid sphere, the good agreement between the corrected drag coefficients and the standard drag curve indicates that at these test conditions the effects of unsteady curvilinear motion on drag are negligible. Consequently, the measured drag coefficients in this experiment are modified by vaporization, but are not significantly affected by unsteady or curvilinear motion.

The Effect of Curvilinear Motion on Droplet Lift

From the same droplet trajectories investigated above, small but non-negligible lift coefficients ($C_L/C_D \approx 0.1-0.15$) are measured in the relatively high droplet Reynolds number ($Re > 20$) and high air temperature cases ($T_{air} > 473$ K). On the other hand, the measured lift coefficients in low droplet Reynolds number and low air temperature cases, where the Reynolds numbers range from 10 to 20, are negligible. Therefore, lift is only measured at Reynolds numbers above that required for the onset of a recirculating wake, i.e. $Re > 20$, and at higher air temperatures, i.e. under vaporizing conditions. In order to demonstrate the effect of lift on droplet trajectories, droplet trajectories are calculated without lift, and then compared with the measured trajectories in Figures 3-a and 3-b. For both cases, drag coefficients are estimated using the drag correlation suggested by Chen and Yuen (1976) and Chiang, Raju, and Sirignano (1992). As shown in Figure 2-b, the evaporating droplet drag coefficients can be reasonably predicted using the Chiang, Raju, and Sirignano's drag correlation. As shown in Figure 3-a, the calculated droplet trajectory agrees well with the measured droplet trajectory. In this case, the range of droplet Reynolds numbers is 10-25, and air temperature is 423 K. On the other hand, as shown in Figure 3-b, the discrepancy between the calculated and measured trajectory is significant, where the droplet Reynolds number ranges from 15 to 38, and air temperature is 473 K. In this case, the difference can be attributed to droplet lift that is not included in the calculation. The magnitude of the lift coefficients and the direction of the lift force in this experiment agree with the results of Odar's experiment (1968) which is based

on a non-vaporizing large solid sphere. Clift, Grace and Weber (1978) suggested that the lift force observed for curvilinear trajectories is due to the development of an asymmetric wake behind the sphere. The present results support this explanation, because the effect of lift is not noticeable until the droplet Reynolds number is greater than that required to obtain a recirculating wake, i.e. $Re > 20$.

Turbulence Effects on Droplet Drag

Figures 4-a and 4-b show the measured droplet velocities from a small dispersion and large dispersion case, respectively. As shown in Figure 4-a, the magnitude of the velocity fluctuation is negligible compared to the average velocity, which allows determination of the average components of droplet acceleration by direct finite differentiation. Under this condition of small dispersion, the drag coefficients are obtained based on the average relative velocity and acceleration. In Figure 4-b, however, velocity fluctuations affect the entire history of droplet velocity, in which case only dispersed trajectory can be investigated.

The experimentally obtained drag coefficients in a low dispersion case are shown in Figure 5. The drag coefficients are up to 80 % greater than the standard drag coefficients at the same Re . The figure also indicates that the drag coefficient increases with increasing relative turbulence intensity and decreasing droplet diameter. Since the pressure drag (form drag), which is determined by wake development behind the droplet, is dominant in this Reynolds number range, the increased drag force can be attributed to the modification of the droplet's wake development by turbulence. The increased drag coefficient in the presence of free-stream turbulence was explained by Clamen and Gauvin (1969). They argued that "turbulence reduces the extent of the separated region behind the body so that the flow in the main stream must turn at a sharper angle. There must be a greater pressure difference between the outer flow and the base region to produce the increased curvature in the streamlines; and, since the free-stream pressure is fixed, the base pressure must be lower.

References

- Chen, L.W. and Yuen, M.C. (1976) *Combust. Sci. Technol.* 14, 147-154
 Chiang, C.H., Raju, M.S. and Sirignono, W.A. (1992) *Int. J. Heat Mass Trans.*, 35, 1307
 Clamen, A. and Gauvin, W.H. (1969) *A.I.Ch.E.*, vol 15, No. 2, 184-189
 Clift, R., Grace, J.R., and Weber, M.E. (1978) *Bubbles, Drops, and Particles*. Academic Press, New York.
 Odar, F. (1968) *J of Appl. Mech.*, 90, 238
 Torobin, L.B. and Gauvin, W.H. (1961) *A.I.Ch.E.*, Vol. 7, No. 4, 615
 Videto, B.D. and Santavicca, D.A. (1991) *Comb. Sci. and Tech.*, Vol 76, 159-164

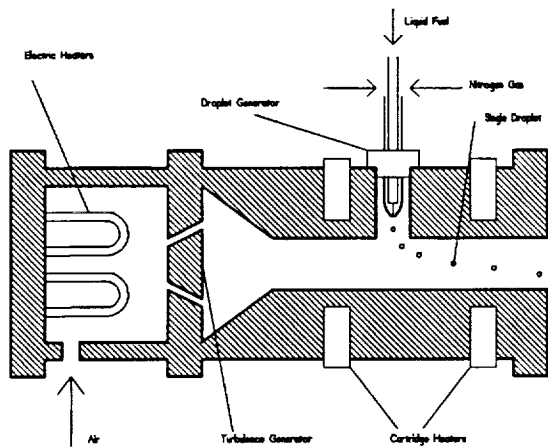


Figure 1. Schematics of Experimental Apparatus

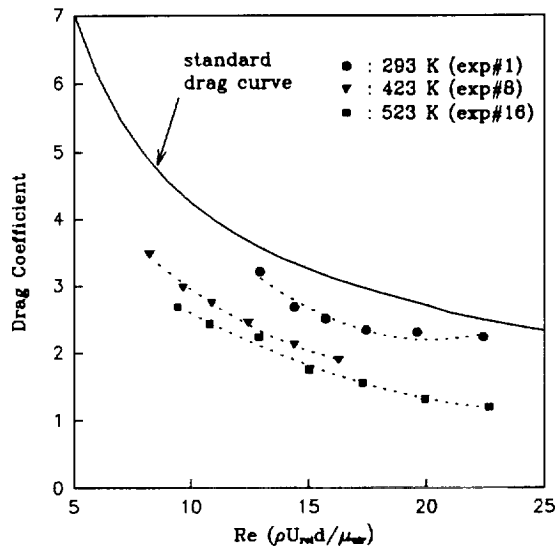


Figure 2-a. Measured drag coefficients at different temperatures

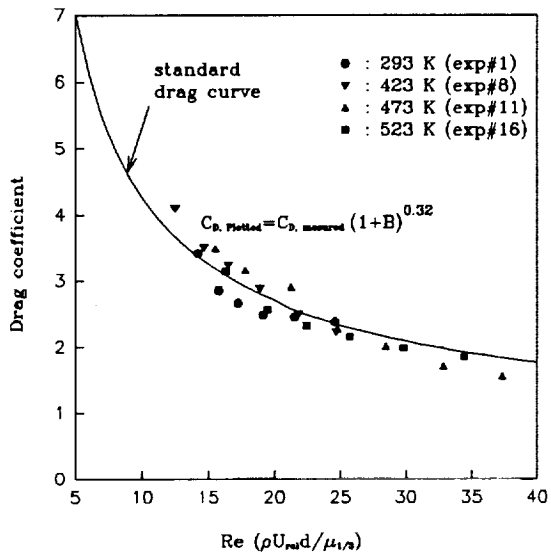


Figure 2-b. Correlated drag coefficients at different temperatures

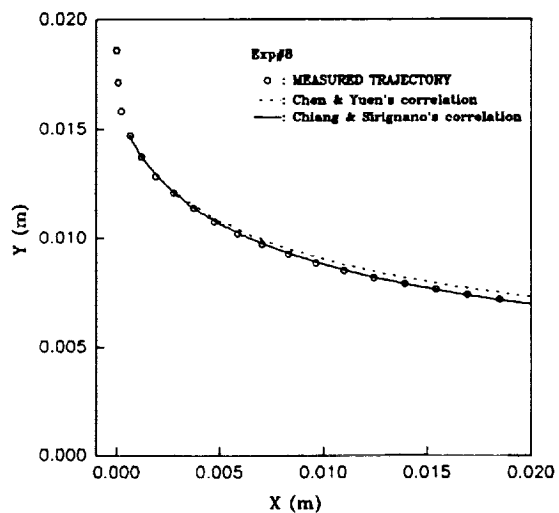


Figure 3-a Measured and Calculated Droplet Trajectories of Experiment #8

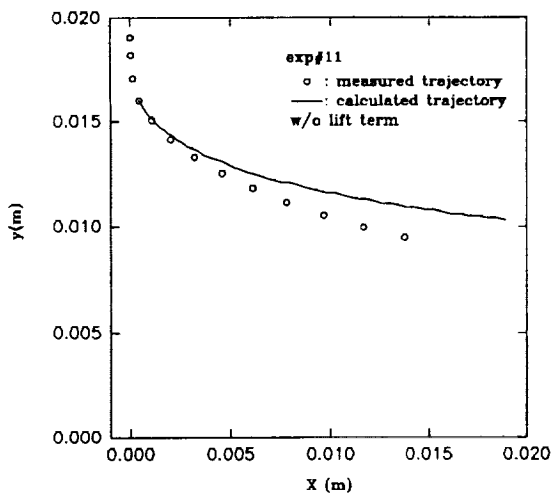


Figure 3-b. Measured and Calculated Droplet Trajectories of Experiment #11

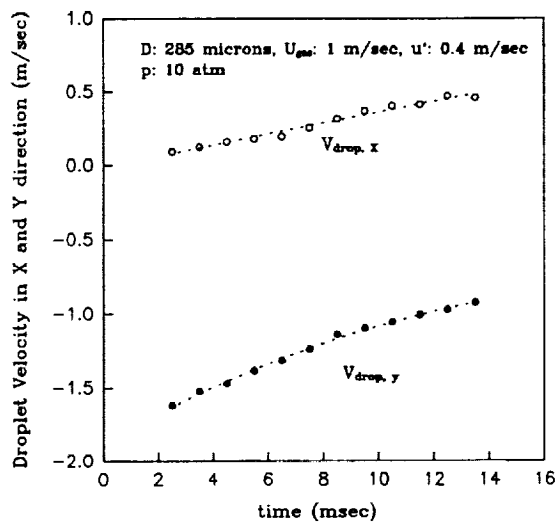


Figure 4-a. Droplet velocity with negligible velocity fluctuation

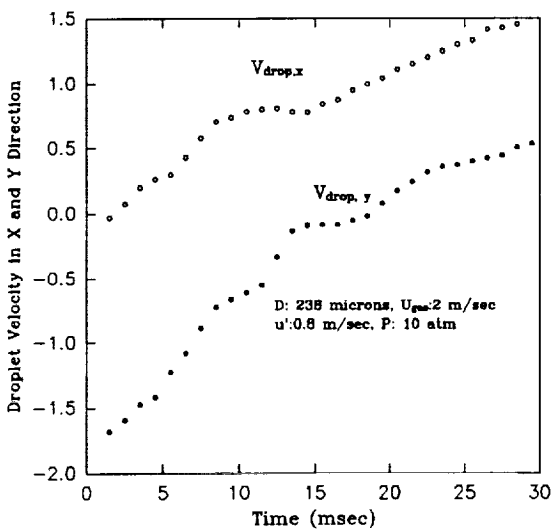


Figure 4-b. Droplet velocity with large velocity fluctuation

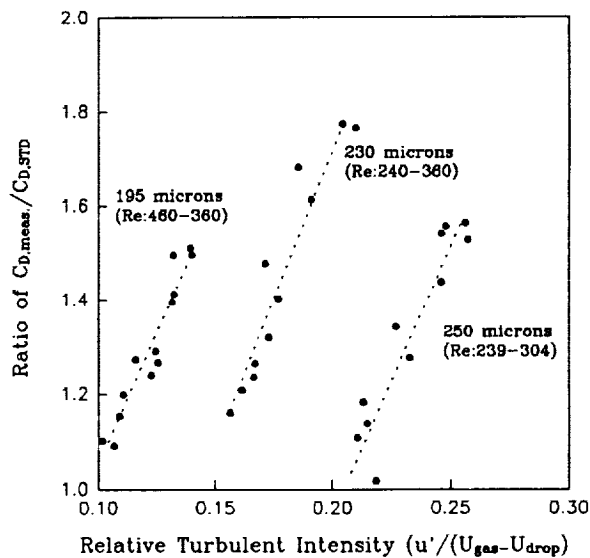


Figure 5. Measured drag coefficients with relative turbulence intensity

Droplet Vaporization in an Acoustic Field (M.S. Ondas)

Combustion instabilities are still a major problem in the operation of liquid propellant rocket engines. The instabilities are caused by the complex interactions between the fluid dynamics and the combustion process and can be very destructive. They are generally classified according to the frequency of the instability. Low frequency combustion instabilities, commonly referred to as chug, are on the order of 10-200 Hz and are generally the result of pressure oscillations in the injector feed system. High frequency instabilities are those with frequencies of 1000 Hz and higher, and these are linked with the combustion process and the acoustical resonances of the combustion chamber itself. The third class of instabilities are those of intermediate frequencies which lay in the loosely defined range between low and high frequency instability. These can be caused by mechanical vibrations, coupling with the feed system, or by various other system fluctuations. The low and intermediate frequency instabilities are the least likely to cause structural damage, and they are also understood the best.^{1,2}

It is unfortunate that the high frequency instabilities are so poorly understood. These instabilities are the most destructive and can cause excessive system vibration or drastically increased local heat transfer rates that can lead to engine meltdown. Methods for dealing with these instabilities include the use of injector baffles and/or acoustic damping devices in the combustion chamber. This cut-and-try approach has worked in the past to stabilize engines, but it was used as a fix to eliminate the problem after the design phase. The ideal situation would be to understand the mechanisms that initiate and sustain these high frequency instabilities and eliminate their causes, rather than just apply costly fixes during the manufacturing process of the engine.²

In recent years, there has been much discussion about what mechanisms may be responsible for the high frequency instabilities. During the JANNAF sponsored workshop on Liquid Rocket Engine Combustion Driven Instability Mechanisms,³ five categories of basic combustion physics were identified: fluid mechanics, injection, atomization, vaporization, and mixing. These mechanisms were discussed and then ranked according to how important each is likely to be to the instability process. Each mechanism must be thoroughly investigated in its own right to determine its actual relevance to the problem at hand. Vaporization was considered to be a priority issue in both the subcritical and supercritical regime. Fundamental data on the vaporization process is critical for basic physical understanding as well as for providing a database for analytical and computational models.

The objective of this research is to study droplet vaporization in the presence of an acoustic wave. Specifically, the determination of what conditions allow the vaporization process to be driven by an acoustic wave. The amplitude as well as the frequency of the imposed acoustic field will be investigated. This will yield information as to when an instability can be initiated or amplified by a small disturbance. In order to study the vaporization process as it relates to combustion instability, it must first be separated from other possible mechanisms such as atomization. This must be done to separate possible coupling effects between the two mechanisms.

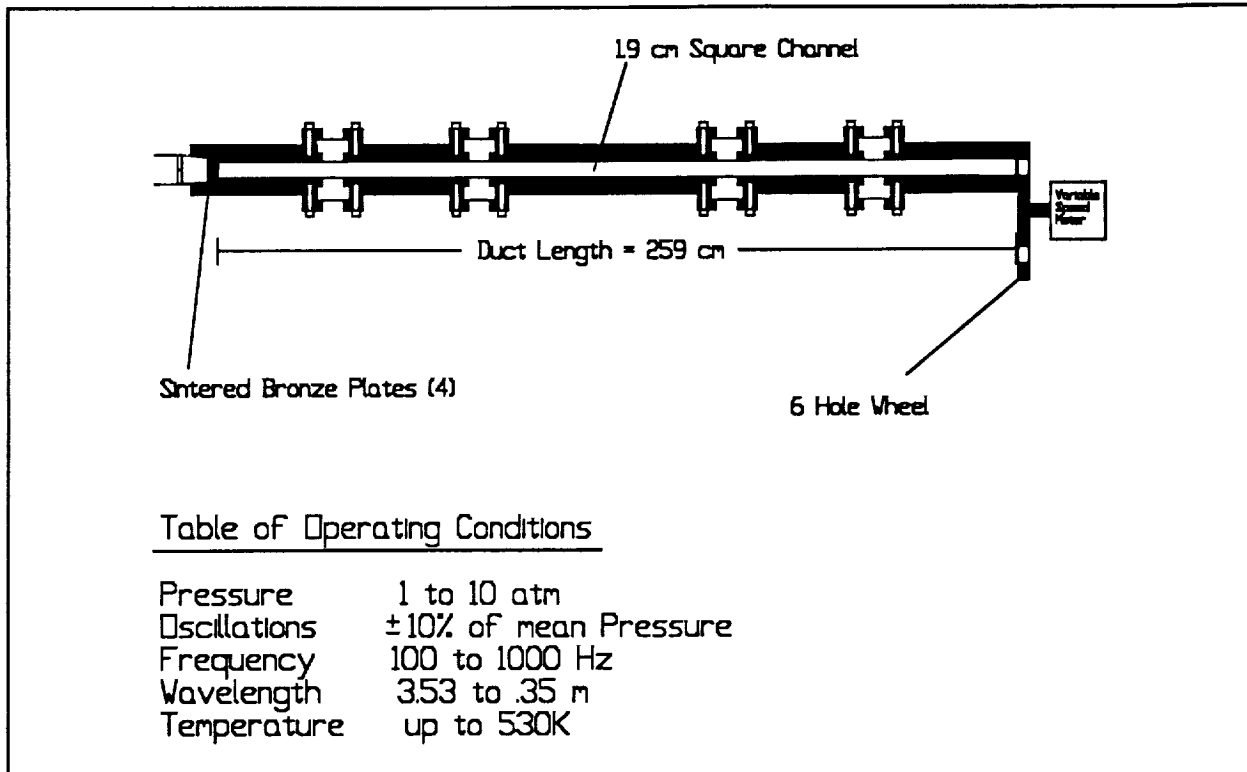


Figure 1 Schematic drawing of the resonant duct

A test section expressly for this purpose has been constructed in the Turbulent Combustion Laboratory at The Pennsylvania State University and is shown schematically in Figure 1. The test section is a square channel 1.9 cm on a side with a length of 259 cm. The square cross section was utilized to facilitate optical access. The test section is capable of operating at pressures up to 10 atm. at a temperature of up to 530 K with mean cross flow velocities of up to 10 m/s. The unique feature of this test section is that an acoustic wave in the frequency range from 100 to 1000 Hz at amplitudes of approximately $\pm 10\%$ of the mean pressure can be produced in the duct. This is done by placing a six-orifice rotating wheel at the end of the duct to periodically open and close the exit port. By adjusting the rotational speed of the wheel, a specific longitudinal resonance of the duct can be excited.

In order to obtain single droplets, a syringe feed system is used to maintain a constant size droplet at the end of a small diameter piece of stainless steel tubing (.018" OD, .013" ID). A .010" thermocouple runs down the length of the tube to facilitate measurement of the drop temperature. The feed rate to the droplet is controlled by a variable voltage DC motor turning a micrometer mounted above the syringe. By using various gearing ratios, a very wide range of feed rates is attainable to match a wide range of vaporization rates. A schematic representation of this setup is shown in Figure 2.

Currently, two different methods are being utilized to image the droplet and its surrounding vapor wake. Both techniques use planar laser induced fluorescence, and each has some specific advantages and disadvantages. The first method is an exciplex-based vapor/liquid visualization technique, and the second is an

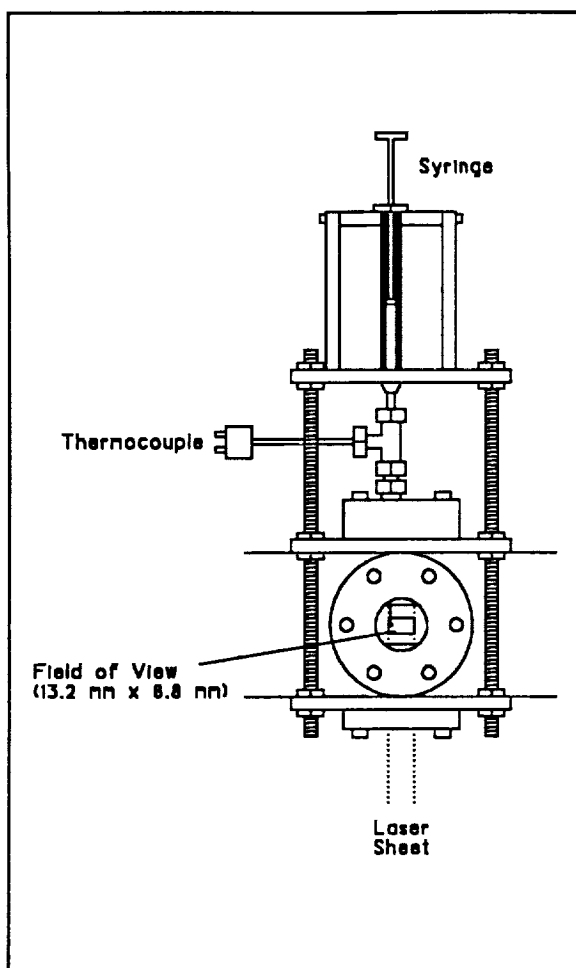


Figure 2 Schematic drawing showing optical port with syringe feed system (excluding the motor drive)

acetone fluorescence technique.

The exciplex-based vapor/liquid fluorescence technique uses chemical dopants to act as a marker for the fuel itself. The base fuel used in the experiments was tetradecane, and the chemical dopants used were TMPD and 1MN. This is the same exciplex scheme that was described previously in the exciplex thermometry section of the report, the only difference being the concentration of the dopants which were added. The mixture used was 1% TMPD, 9% 1MN and 90% tetradecane by weight. With these concentrations, the temperature dependence is removed from the exciplex reaction. In the liquid phase, the exciplex reaction proceeds to completion due to the high concentration of 1MN present. Thus, the liquid phase is dominated by green (500 nm) fluorescence from the exciplex. In the vapor phase the exciplex is unstable, so the vapor is marked by the blue (400 nm) fluorescence from the monomer (TMPD); therefore, the fluorescence from the two phases is spectrally separated.⁴⁻⁶

In the most recent experiments, vaporizing droplets were suspended from the end of the tubing and immersed in a nitrogen crossflow to prevent the strong quenching effects due to molecular oxygen. The droplet and its vapor wake were then illuminated using either the 355 nm (3rd harmonic) or 266 nm (4th harmonic) beam from an Nd:YAG laser. The flow conditions were 1.3 m/s at 220°C and a pressure of 7.8 atm. The vapor image was obtained using a Corion S-25-400R bandpass filter (400 nm, 25 nm FWHM) in front of a Princeton Instruments intensified CCD array camera. This technique provided some images of the vapor wake, but the signal to noise ratio obtained was lower than expected. One reason for this may be the presence of small quantities of oxygen in the nitrogen, and this possibility is currently being investigated. Another reason may be the low concentration of fuel vapor in the wake. A higher concentration of fuel vapor, e.g. higher vaporization rates, would yield higher signal levels. Since the test section is near its maximum temperature capability, an increase in temperature is not a feasible solution. One way to produce higher vaporization rates is to use a more volatile fuel.

The second fluorescence technique uses acetone as a fuel. Acetone is a very volatile fluid (boiling point 56°C) and it also fluoresces and phosphoresces upon ultraviolet laser excitation.⁷ The latest acetone experiments were similar to those performed with the tetradecane based exciplex mixture. Acetone droplets

were suspended from the small tubing and immersed in a nitrogen crossflow. Once again, nitrogen was used to minimize the effects of oxygen quenching. The flow conditions used were a mean velocity of 1.2-1.5 m/s at temperatures of 50-85°C and a pressure of 6.4 atm. The fourth harmonic (266 nm) of an Nd:YAG laser was used as the excitation source. Images were once again recorded using the Princeton Instruments intensified CCD array camera. Since the fluorescence is broadband (350 nm - 550 nm), only a 385 nm high-pass filter was used to eliminate elastic scattering at the laser wavelength (266 nm).

The images obtained using the laser induced acetone fluorescence were of higher quality than those obtained with the exciplex fluorescence technique. At this point it is premature to assume that an increase in fuel volatility is the primary reason for the improved image quality. Until the oxygen quenching problem can be addressed in the exciplex technique, neither method will be deemed to be the better technique.

The upcoming experiments to be performed will address potential problems that have been encountered and also aim to increase the signal strength obtained from both of the techniques. In an effort to increase laser power, a new set of deep UV grade synthetic quartz windows has been purchased to allow for a higher percentage of the incident laser energy to penetrate into the test section. Also, to eliminate the disruption in the flowfield caused by the tubing, experiments with falling drops will be initiated. Once the data acquisition system is more fully developed and images are of sufficient quality, an acoustic field will be imposed on the mean gas flow and droplet vaporization in the presence of an acoustic wave will be studied.

References

1. Sutton, George P., Rocket Propulsion Elements, pp. 184-193, John Wiley & Sons, New York, 1986.
2. Harrje, D.T. and Reardon, F.H. (editors), Liquid Propellant Rocket Combustion Instability, NASA SP-194, 1972.
3. Jensen, R.J., "A Summary of the JANNAF Workshop on Liquid Rocket Engine Combustion Driven Instability Mechanisms", presented at the 26th JANNAF Combustion Meeting, Pasadena, CA, October, 1989.
4. Melton, L.A. and Verdick, J.F., "Vapor/Liquid Visualization in Fuel Sprays", Twentieth Symposium (International) on Combustion/ The Combustion Institute, pp. 1283-1290, 1984.
5. Melton, L.A., "Spectrally Separated Fluorescence Emissions for Diesel Fuel Droplets And Vapor", Applied Optics, Vol. 22, No. 14, 1983.
6. Rotunno, A.A., Winter, M., Dobbs, G.M., and Melton, L.A., "Direct Calibration Procedures for Exciplex-Based Vapor/Liquid Visualization of Fuel Sprays", Combustion Science and Technology, Vol. 71, pp. 247-261, 1990.
7. Lozano, Antonio, "Laser-Excited Luminescent Tracers for Planar Concentration Measurements in Gaseous Jets", HTGL Report No. T-284, Mechanical Engineering Department, Stanford University, August 1992.

Publications

The following publications are based on work done under this grant.

Santavicca, D. A. and Coy, E. B., "A Double-Pulse, Planar, Fluorescence Imaging Technique for Studying Droplet-Turbulence Interactions in Vaporizing Sprays," 27th JANNAF Combustion Meeting (1990).

Song, Y.-H. and Santavicca, D. A., "An Experimental Study of Droplet Dispersion in Turbulent Flows," 28th JANNAF Combustion Meeting (1991).

Coy, E. B. and Santavicca, D. A., "Simultaneous Droplet Velocity and Size Measurements in Fuel Sprays," SAE Paper No. 912399, 1991 SAE Fuels and Lubricants Meeting (1991).

Song, Y.-H. and Santavicca, D. A., "An Experimental Study of Drag and Lift Forces Acting on an Evaporating Droplet Along a Curvilinear Trajectory," Eastern States Section of The Combustion Institute Fall Meeting (1993).

Song, Y.-H. and Santavicca, D. A., "An Experimental Study of Droplet Motion in a Highly Turbulent Flow," Eastern States Section of The Combustion Institute Fall Meeting (1993).

Personnel

D. A. Santavicca, Principal Investigator

Y.-H. Song, Ph.D. Student (supported by this grant)

E. B. Coy, Ph.D. Student (supported by NASA Propulsion Center and AFOSR AFRAPT Fellowship)

T. D. Spegar, Ph.D. Student (supported by NASA Propulsion Center and DoD AASERT Fellowship)

S. C. Greenfield, Ph.D. Student (supported by AFOSR AFRAPT Fellowship)

M. S. Ondas, Ph.D. Student (supported by NASA Propulsion Center)

M. R. Hayner, Undergraduate Student